Polyester/SiO_2 Nanocomposites: Gas Permeation, Mechanical, Thermal and Morphological Study of Membranes

Ahmadizadegan, Hashem*[+]

Department of Chemistry, Darab Branch, Islamic Azad University, 7481783143-196, Darab, I.R. IRAN

ABSTRACT: *Using of nanocomposite membranes composed of polymer and inorganic nanoparticles is a novel method to enhance gas separation performance. In this study, membranes were fabricated from polyester (PE) containing silica (SiO_2) nanoparticles and gas permeation properties of the resulting membranes were investigated. Morphology of the membranes, SiO_2 distribution and aggregates were observed by Scanning Electron Microscopy (SEM) and Transmission Electron Microscopy (TEM) analysis. Furthermore, thermal stability, the residual solvent in the membrane film, and structural ruination of membranes were analyzed by ThermoGravimetric Analysis (TGA). The effects of SiO_2 nanoparticles on the glass transition temperature (T_g) of the prepared nanocomposites were studied by Differential Scanning Calorimetry (DSC). The results obtained from gas permeation experiments with a constant pressure setup showed that adding SiO_2 nanoparticles to the polymeric membrane structure increased the permeability of the membranes.*

KEYWORDS: *Polyester; Nanocomposite; Silica; Thermal stability; Gas Permeation.*

INTRODUCTION

Polymer–inorganic hybrid nanocomposites are an emerging class of materials that hold significant promise due to their outstanding properties, which usually arise from a combined effect of the properties of their polymeric and inorganic components [1]. Nanoparticles and nanocomposites are used in a wide range of applications comprising of diverse fields, such as medicine, textiles, cosmetics, agriculture, optics, food packaging, optoelectronic devices, semiconductor devices, aerospace, construction, and catalysis [2–4]. Polymeric nanocomposites consisting of inorganic nanoparticles and organic polymers represent a new class of materials that exhibit improved performance compared to their microparticle counterparts [5]. Organic-inorganic hybrid has received much attention and has been extensively studied for a long time as a new class of high-performance materials which offer the advantages of both an organic polymer (e.g., flexibility, dielectric, ductility, and processability) and an inorganic material (e.g., rigidity, thermal stability) [8,9]. We define the terms of "hybrid" and "composite" as following: "hybrid" materials are those that have strong chemical interaction between organic and inorganic components such as covalent bonds, and "composite" materials are those that show weak or no interactions between the two components.

Silica nanoparticles are gaining considerable interest for a wide variety of applications in various fields of material science like electronic, chemical, optical and mechanical industries due to their unique and promising

** To whom correspondence should be addressed.*
+ E-mail: h.ahmadizadegan.2005@gmail.com ; h.ahmadizadegan@ch.iut.ac.ir
1021-9986/2020/2/33-47 15/$/6.05

physical and chemical properties [6]. The surface modification of nanoparticles in order to change their physical and chemical properties has become an area of significant research in industry. However, the applications of silica nanoparticles are largely limited because of their high energetic surface, which causes the silica nanoparticles to be easily agglomerated. However, this problem could be resolved by using surface modification methods [7]. Surface modification of silica nanoparticles has attracted attention because it produces excellent integration and an improved interface between nanoparticles and polymer matrices [8]. Polymer matrices reinforced with modified silica nanoparticles combine the functionalities of polymer matrices, which include low weight and easy formability, with the unique features of the inorganic nanoparticles.

However, the nanoparticles have a strong tendency to undergo agglomeration in the polymer matrix, degrading the mechanical properties of the nanocomposites [9]. To improve the dispersion stability of nanoparticles in polymer, it is essential that the particle surface be modified by reactive surface functionalities to generate a strong interaction between monomer precursors and particle surface and repulsion between particles. In order to precisely design desirable surface functionalities, one can select an appropriate surface modification method according to the needs in terms of polymer functional groups and composition.

Synthesizing polyester (PE) containing silica (SiO_2) nanoparticles hybrid and composite materials and investigating their physical and gas transport properties have also received much attention [10]. PE/SiO_2 hybrids can be prepared by sol-gel processes or the addition of colloidal silica. Generally, it is said that colloidal silica has a dense structure and silica prepared via the sol-gel reaction has an amorphous three-dimensional network structure with nanopores [11].

The dispersion of silica components in the PE matrix has a significant impact on the properties of hybrids and composites. The modification of PE molecular terminals is one of the most effective methods to enhance the compatibility between PE and silica and, thereby, to improve the dispersibility of the silica components [12].

Polymer matrix should usually have several properties such as chemical stability, biocompatibility and chemical function-alities [13]. Chiral polyester can be a good candidate for these purposes, because of their significant properties such as high thermal stability, mechanical strength, good chemical resistance, high biodegradability and flexibility [14].

This study reports the influence of SiO_2 nanoparticles on the structural characteristics and the gas permeability of PE polymer membranes. SiO_2 is one of the metal oxides used for enhancing strength and thermal resistance of membranes. It also exhibits good affinity for some gas molecules and can be used as potential metal oxide filler in nanocomposite gas separation membrane preparation. Nanocomposite membranes were fabricated by the solution casting method with different loadings of SiO_2 nanoparticles. Particle dispersion and morphology of the prepared nanocomposite were characterized using scanning electron microscopy (SEM), and transmission electron microscopy (TEM) techniques. Characteristics of membranes such as thermal degradation and glass transition temperature (T_g) were evaluated by TGA and DSC. Gas permeation properties of CO_2, CH_4, N_2, and H_2 are reported as a function of particle concentration.

EXPERIMENTAL SECTION

Materials and characterization

4-(trifluoromethyl) phenol, 1-chloro-4-nitrobenzene, L(-)-tartaric acid, and tetrahydrofuran (THF) were obtained from Guoyao Chemical Plant (Shanghai, China). Dimethylacetamide (DMAc) and N, N-Dimethyl-formamide (DMF) was provided by Shanghai Gaoqiao Petrochemical Co. (Shanghai, China). Amorphous nanosilica powder was obtained from Neutrino (Tehran, Iran) with an average particle size of 10–15 nm and 99.99%purity.

Infrared spectra of the samples were recorded at room temperature in the range of 4000–400 cm–1, on (Jasco-680, Japan) spectrophotometer. The spectra of solids were obtained using KBr pellets. The vibrational transition frequencies are reported in wave numbers [cm^{-1}]. Band intensities are assigned as weak (w), medium (m), strong (s) and broad (br). Proton nuclear magnetic resonance (^{1}H-NMR spectra, 500 MHz) was recorded in N, N′-dimethylsulfoxide (DMSO)-d_6 solution using a Bruker (Germany) Avance 500 instrument. Multiplicities of proton resonance were designated as singlet (s) and multiplet (m). Inherent viscosity was measured by a standard procedure with a Cannon-Fenske (Mainz,

Germany) routine viscometer. Specific rotation was measured with a Jasco (Osaka, Japan) P-1030 polarimeter at the concentration of 0.5 g/dl at 25ºC. TGA data were taken on STA503 WinTA instrument in a nitrogen atmosphere at a heating rate of 10ºC/min. Elemental analyses were performed by Leco, CHNS-932. Gel permeation chromatography (GPC) was performed with a Waters instrument (Waters 2414) and tetrahydrofuran (THF) was used as an eluent (flow rate 0.5 mL/min). Polystyrene was used as a standard and a RI detector was used to record the signal in GPC. X-ray diffractometer (Philips Xpert MPD, Germany) with Cu Ka radiation (λ = 1.540 Å) was employed to determine the structure of newly synthesized polymers. Bragg angles ranged from 10–80° at the speed of 0.051min^{-1}. The operating current and voltage were maintained at 30 mA and 40 kV, respectively. The size distributions of the PE/SiO_2 were measured by the nanoparticle tracking analysis (NTA, Nano Sight LM20). The NTA is a powerful tool to obtain the average statistical data of the sample0 s dimension, which based on the correlation between the sample size and the corresponding Brownian motion velocity under a certain temperature and viscosity of the disperse phase. In this study, the disperse phase was ultrapure water, with 20 1C. The morphology observation was performed with FEI QUANTA-400F scanning electronic microscope (SEM).The permeation cell was placed in a thermostatically controlled housing for maintaining isothermal measurement conditions. The reproducibility of the measurements was checked from three independent measurements using the same membrane, and it was better than ±5%.

Synthesis of chiral diol monomer

According previous articles [11, 12] in a 50 ml three-neck round-bottomed flask equipped with a stirring bar under nitrogen atmosphere, 1.00 g (6.13 mmol) of 4-(trifluoromethyl) phenol, 0.99 g (6.14 mmol) of 1-chloro-4-nitrobenzene, (12.38 mmol) of potassium carbonate, and 20 mL of DMAc was added. The solution was stirred at 125 °C for 4 h. After cooling to room temperature, the mixture was pureed into 300 mL of methanol. The precipitate was dried at 55 °C under vacuum and the product was recrystallized from glacial acetic acid to obtain the nitro monomer in 90% yield. In the second step, a mixture of hydrazine monohydrate (3 mL), nitro compound (2.00 g, 7.06 mmol), a catalytic amount of 10% Pd/C (0.15 g), and ethanol (90 mL) was heated at reflux for 15 h. To remove Pd/C, the reaction solution was filtered and purified by recrystallization from methanol and then it was dried in vacuum (80% yields). 4-(4-(trifluoromethyl)phenoxy)benzenamine and the chiral reagent L (-)-tartaric acid were added to DMF under magnetic stirring, and the reaction mixture was heated to 55°C and refluxed for 24 h. After the reaction was completed, the solution containing dihydroxyl groups and the trifluoromethyl group was obtained. For $C_{17}H_{12}F_3NO_5$ monomer the yield is 70–75%. Rotation value ($[\alpha]_D^{25}$) of monomer diol in concentration 4×10^{-2} mg/mL (DMF) is -25.3 **[**11, 12**]**.

FT-IR (KBr, cm^{-1}): 3456(s), 3432 (s), 3118 (w), 3064 (w), 1727 (s), 1625 (s) 1565 (m), 1546 (m) 1,433 (w), 1312 (w), 1122 (w), 840 (m), 650 (w).

^{1}H-NMR (500 MHz, DMSO-d_6, ppm): 4.15 (s, 2H, OH), 4.75 (d, 2H, C-H), 7.16-7.18 (d, 2H, Ar-H, *J*= 4.5 Hz), 7.39-7.41 (d, 2H, Ar-H, *J*= 4.0), 7.73-7.75 (d, 2H, Ar-H, *J*= 3.0),7.95-7.97 (d, 2H, Ar-H, *J*= 2.0).

^{13}C-NMR (125 MHz, DMSO-d_6), δ (ppm): 83.01 (C-O), 119.31 (Ar), 122.61 (Ar), 1266.26 (Ar), 127.22 (CF_3), 130.59 (Ar), 132.22 (Ar), 134.55 (Ar), 137.62 (Ar), 145.85 (Ar), 171.25 (C=O).

Elemental analysis: Calcd. For $C_{17}H_{12}F_3NO_5$ (367.28 g mol^{-1}): C, 55.59%; H, 3.29%; N, 3.81%. Found: C, 55.61%; H, 3.25 %; N, 3.80%.

Polymer synthesis

According previous articles [11, 12] a solution of Py (0.20 mL) with tosyl chloride (TsCl) (0.29 g; 1.55×10^{-3}mol) after 30 min stirring at room temperature, was treated with DMF (0.09 ml; $1.22\cdot10^{-3}$ mol) for 30 min and the mixture was added dropwise to a solution of diacid (0.10 g; $4.63\cdot10^{-4}$ mol) in Py (0.20 mL). The mixture was maintained at room temperature for 30 min and then chiral diol (0.18 g; $4.63\cdot10^{-4}$ mol) was added to this mixture and the whole solution was stirred at room temperature for 30 min and then at 120ºC for 4 h. As the reaction proceeded, the solution became viscous and then the viscous liquid was precipitated in 30 mL of methanol to give 0.94 g pale brown powder PE (90% yield) and the specific rotation was measured in concentration 4×10^{-2} mg/mL (DMF) ($[\alpha]_D^{25}$ = -19.1). The Number average

molar mass (M_n), Mass average molar mass (M_w) and Polydispersity index (M/M_n) of PE is 83287, 155233 and 1.86 respectively.

FT-IR Peaks (KBr, cm^{-1}): 3448 (w, br), 3021 (w), 3060 (w), 2955 (S), 2872 (w), 1775 (s), 1725 (s), 1518 (m), 1372 (s), 1269 (w), 1235 (m), 1196 (m), 1169 (m), 1112 (w), 1099 (w), 737 (m).

^{1}H-NMR (500 MHz, DMSO-d_6, ppm): 5.77 (d, 2H, C-H), 7.51-7.53 (d, 2H, Ar-H, *J*= 4.5 Hz), 7.57-7.59 (d, 2H, Ar-H, *J*= 4.0), 7.63-7.65 (d, 2H, Ar-H, *J*= 3.0),7.72-7.74 (d, 2H, Ar-H, *J*= 2.0), 7.82-7.84 (d, 2H, Ar-H, *J*= 2.0), 7.81-7.83 (d, 2H, Ar-H, *J*= 4.5 Hz), 7.90-7.92 (d, 2H, Ar-H, *J*= 4.0), 8.02-7.04 (d, 2H, Ar-H, *J*= 2.0).

Elemental analysis: Calcd. For $C_{31}H_{22}F_3NO_7$ (577.13 g/mol: C, 64.47%; H, 3.84%; N, 2.43%. Found: C, 64.38%; H, 3.85 %; N, 2.44%.

Preparation of PE membrane

PE solution was prepared by dissolving 15 wt% of PE in DMAc under continuous stirring for 24 hours at 30 °C until the polymer dissolved. Ten minutes before casting, the mixture was sonicated. Then PE films were cast on a clean, dry, level glass plate and after 1 minute evaporating time, membranes were immersed in a water coagulation bath (20 °C) for 24 hr. Finally membrane was dried in an oven at 70 °C about 6 hours to remove the remained solvent and water from the coagulation bath [11].

Preparation of PE/SiO_2 nanocomposite membranes

The nanocomposite membranes were prepared by addition of SiO_2 nanoparticles in different amount (5, 10, 15 wt%) to the polymer solution. First SiO_2 nanopowder was dispersed in DMAc under continuous stirring for about 4 hours followed by sonication for 5 min to break up any aggregation and improve the dispersion quality. Then polymer was gradually added up to 15 wt% concentration and the stirring was continued for 24 hours to achieve a homogenous solution. After that, membranes were cast in the same way as for pure PE membrane. PE/SiO_2 membranes for gas permeation test were prepared by solution casting. The typical procedure is as follows: a homogeneous DMAc solution containing ~9% (w/v, g/mL) polymer was filtered through a 0.38 μm PTFE filter and quickly casted onto a clean and leveled glass plate. The solution was heated under an infrared lamp at about 80 °C for 2 days to slowly evaporate the solvent. The obtained isotropic film was further dried at 160 °C under vacuum overnight, and then soaked in methanol for 6 h to remove the residual DMAc and casting history, finally dried at 120 °C under vacuum for 12 h. Thermogravimetric analysis (TGA, Pyris TG 2000) was used to confirm that all membranes did not contain any residual solvent. The thickness (30–70 μm) of films was measured by digital display thickness gauge (exploit 220200, 1 μm resolution) and the effective area for membrane permeation test was determined by digitally analyzing the scanned image of the permeation sample [15].

Gas Permeability Measurement

The pure gas (N_2, O_2, CH_4 and CO_2) transport properties of prepared membranes were determined using a constant volume/variable pressure method as described in detail by Pye et al. [16]. The feed side gas pressure was 10 bar (gauge) and the active area of the membrane cell was 13.1 cm^2. The specifications of the constant volume/variable pressure setup are also described in detail elsewhere. The gas permeability of membranes was calculated using the following equation:

$$P = \frac{273.15V}{76p_0AT}\frac{dp(t)}{dt}$$

Where P is the permeability in barrer (1 barrer=1×10^{10} cm^3 (STP) cm/cm^2 s cmHg), V, the volume of the down-stream chamber (cm^3), A, the effective membrane area (cm^2), L, the membrane thickness (cm), T, the experimental temperature (K), dp(t)/dt, the steady rate of pressure measured by a pressure transducer in the down-stream chamber and p_0, the feed pressure with the same unit of p(t). The diffusion coefficient (D) was calculated by the time-lag method as below:

$$D = \frac{L^2}{6\theta}$$

Where θ is the time lag (s), the intercept obtained from extrapolating the linear region of the p (t) versus the time plot to the time axis D is the diffusion coefficient (cm^2/s).

The solubility coefficient (S) (cm^3 (STP)/cm^3 cm Hg) was calculated as:

$$S = \frac{P}{D}$$

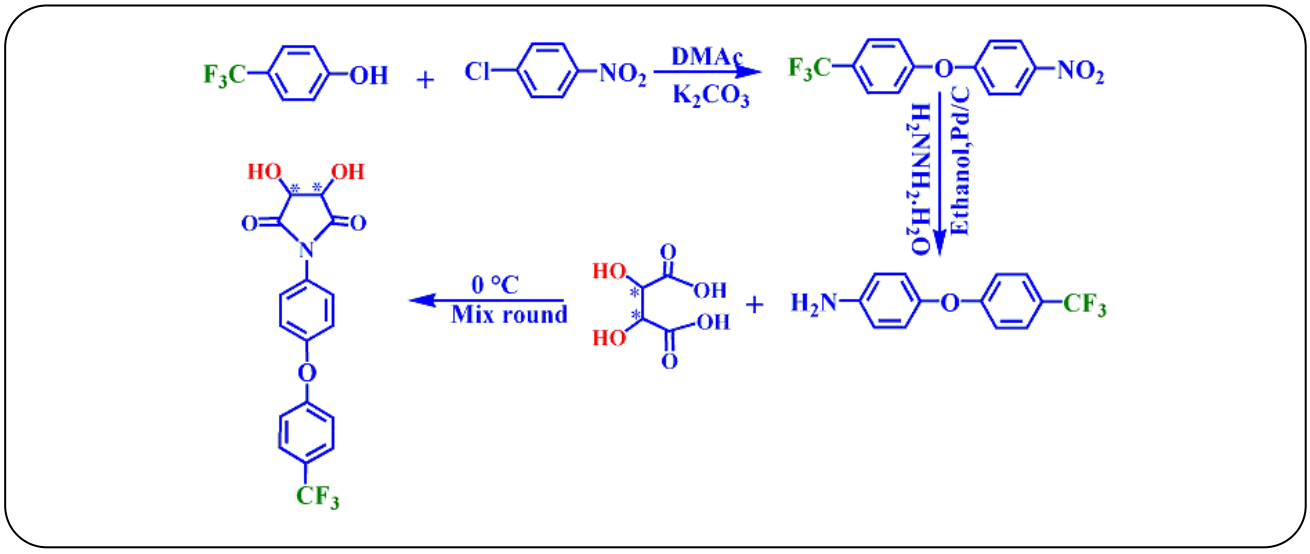

Scheme 1: Synthesis of diol monomer.

The ideal selectivity of membranes ($\alpha_{A/B}$) was determined from pure gas permeability as follow:

$$a_{A/B} = \frac{P_A}{P_B}$$

RESULTS AND DISCUSSION

Synthesis and characterization of chiral diol monomer

Scheme 1 explains the synthetic method for chiral diol using a two-step process. The chemical structure of the synthesized chiral diol was confirmed by elemental analyses (reported in the experimental section), FT-IR, ^{1}HNMR and ^{13}CNMR spectroscopy techniques. In the ^{1}H-NMR spectrum of the chiral diol, the aromatic protons appeared in the range of 7.16–7.97 ppm, and the hydroxyl groups appeared at 4.15 ppm. Moreover, the chiral hydrogen's were observed at 4.75 ppm. In the spectrum of chiral diol (Fig. 2A), the characteristic bonds of amino groups at 3456–3432 cm^{-1}(O–H stretching vibrations) and 840 cm^{-1} (O–H out of plane bending) appeared. In ^{13}C NMR spectrum of chiral diol the aromatic carbons are presented in the range of 119.31–171.25 ppm and the carbon of chiral is appears at around 83.01 ppm [11, 12].

Preparation and characterization of the polyester

The chiral PE was prepared by the one/pot, high/temperature solution polymerization of diacide monomer with aromatic chiral diol at 120 ºC (Scheme 2). The resulting PE showed inherent viscosity 0.94 dL/g at a concentration of 0.5 g/dL. Moreover, the number average molecular weight (M_n), weight average molar weight (M_w) and polydispersity index (PDI) (reported in the experimental section) of the synthesized polymer were further supported by GPC measurements. The FT-IR spectra of the PE conforms that the characteristic absorption bands of the (C=O ester and imide absorption at 1775, 1725 cm^{-1} and 1353 (C–N stretching) and 702 cm^{-1} (C=O bending). The ^{1}H NMR spectrum of the PE exhibits, in which all the peaks have been readily assigned to the hydrogen atoms of the repeating unit and no hydroxyl or acid protons at 10–12 ppm appears, indicating that complete polymerization of PE. Moreover, the peaks at around 4.15 ppm corresponding to the hydroxyl groups in the ^{1}H-NMR spectrum of diol disappeared completely in the ^{1}H-NMR spectrum of the polymer. The PE was also characterized by elemental analysis techniques, and the results are in good agreement with the calculated ones for the proposed structures (reported in the experimental section). These results in sum confirmed the successful formation of the new chiral PE.

FT-IR Analysis of PE/SiO2 nanocomposite membranes

Structural characterization of the pure PE membrane and the PE/SiO_2 nanocomposite membranes was investigated by FT-IR analysis (Fig 1A). The characteristic peaks of symmetric C=O stretching and asymmetric C=O stretching of the ester and imide group were clearly visible at around 1720 and 1777 cm^{-1}.

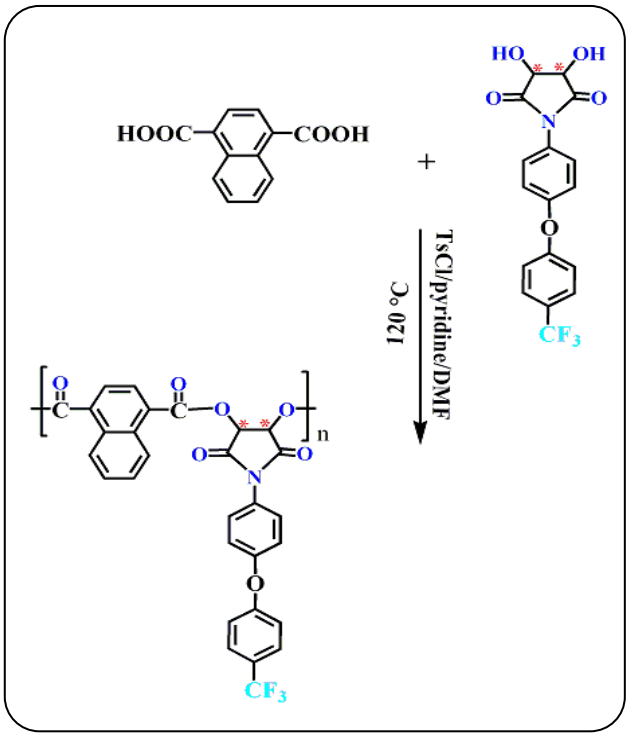

Scheme 2: Synthesis of PE.

The mentioned peaks were the characteristic absorption of ester group as shown in the spectra of the entire pure PE film and PE/SiO_2 nanocomposite films. Besides, the introduction of the SiO_2 led to a broad and strong absorption band in approximately 800 to 400 cm^{-1}. Moreover, the appearance of absorptions at 1100 and 830 cm^{-1} indicated the formation of silicon oxygen bonds in the nanocomposites. Absorption band at 1104 cm^{-1} was attributed to the Si-O-Si stretching and Si-O in NCs obtained. The spectrum of nano-SiO_2 exhibits a wide peak at 3434 cm^{-1}, which is attributed to the O–H stretching [18]. The intense absorption peak at 1089 and 469 cm^{-1} arises from the Si–O–Si stretching and bending vibration, respectively. The peaks of imide rings are at 1711 cm1 for C=O symmetric stretching and 1777 cm^{-1} for C=O asymmetric stretching in the spectrum of pure PE. The characteristic peaks of imide rings can also be found in PE/SiO_2 nanocomposites. In addition, it can be observed that the peak intensities of Si–O–Si stretching with a sign of being overlapped with the peaks of PE in the 1000–1100 cm^{-1} region and bending vibration are enhanced gradually with increasing the nano-SiO_2 contents. These results confirm the presence of SiO_2 NPs in the PE matrix.

X-ray diffraction of NCs

XRD analysis is an experimental method to characterize the phase structure of the materials. Due to its ease of use and availability, X-ray diffraction is most commonly applied to probe the morphology of the polymer and NCs. The XRD patterns of pure PE, SiO_2 NPs and PE/SiO_2 NC (5, 10 and 15 wt%) are shown in Fig. 1B. The XRD patterns of pure PE showed that the polymer was amorphous. Also, XRD pattern revealed that SiO_2, and PE/SiO_2 NCs were amorphous. X-ray diffractgram of nanofiller illustrated an amorphous diffraction pattern. As shown in the Fig. (1 B), after nanofiller was dispersed into the PE matrix, the general shape of the XRD pattern of PE/NCs remains without changed. It could be observed that there was a lack of any sharp diffraction peak in the range of 2θ angle, and these materials illustrated an amorphous nature too. The XRD patterns of pure SiO_2, pure PE, and the NCs are shown in Fig. 1B. In the pattern of pure SiO_2, the lack of any sharp diffraction peak in the range of 2θ angle is attributed to the amorphous nature of this material. A similar pattern can be observed for the pure PE. Fig. 1B represents the XRD patterns for the pure PE and the PE/SiO_2 NC films. In the XRD pattern of the pure PE (Fig. 1(B)), a peak with high intensity appeared around 2θ =20°. The pure PE showed a semicrystalline structure due to the strong intermolecular and intramolecular hydrogen bonding between the PE molecular chains. As can be seen, the XRD patterns of the PE/SiO_2 NC films showed similar behavior to the pure PE.

Furthermore, ED's results of films were further analyzed on the abrasion mechanism with corresponding results shown in Fig. 2. Meanwhile, smart quant results of films were summarized in Table 1. The main components of films contain C, O, Si, The existence of C, O and Si implies that the debris of PE/SiO_2 nanocomposites [18].

Thermal stability of NCs

The TGA curves of the pure PE and fabricated NC films are shown in Fig. 3 and the resulting TGA data are summarized in Table 2 that including temperatures at which 10% (T_{10}) degradation occurs and the residue at 800 °C. TGA has been used under nitrogen atmosphere at a heating rate of 10 °C min^{-1}. The initial decomposition temperatures of the NCs with different SiO_2 nanoparticles

Table 1: EDS result summary for nanocomposite films.

Sample	C (Wt%)	Si (Wt%)
PE/SiO_2 (5%)	69.75	3.25
PE/SiO_2 (10%)	72.36	8.29
PE/SiO_2 (15%)	62.54	13.28

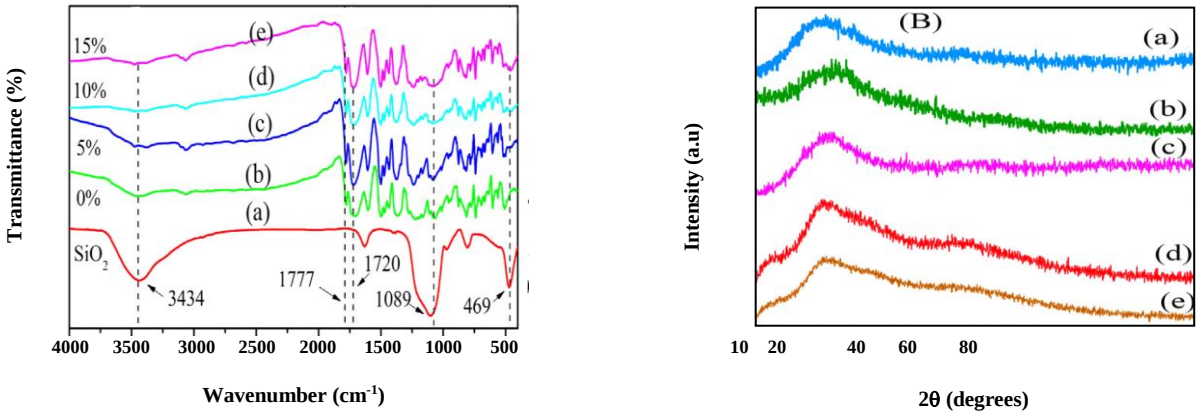

Fig. 1: (A) FT-IR spectra of the pure SiO_2 (a) pure PE (b) PE/SiO_2 NC 5%, (c) PE/SiO_2 NC 10%, (d) PE/SiO_2 NC 15%, (e), (B) XRD patterns of pure SiO_2 (a), pure PE (b) and NC hybrid film with different amounts of SiO_2 nanoparticle (c, d, e).

(5, 10 and 15%) are above 396 °C. The residue at 800 °C of the NCs is higher thermal stability than that of pure PE. Increasing in the thermal stability in NCs is attributed to the high heat resistance exerted by the SiO_2, because the SiO_2 nanoparticles have high thermal stability so coupling of SiO_2 nanoparticles can improve the thermal stability of the NCs. By comparison of the thermal properties of these hybrid materials with different NCs with similar structures [19], the results show that these hybrids had higher thermal stability because of the good interaction between the polymers with hydroxyl groups of SiO_2 nanoparticles. The glass transition temperatures (T_g) values of the polymer matrix and NCs were determined using DSC analysis which showed the rising trend with the increasing of SiO_2 percentage as summarized in Table 3. The restriction of segmental movement due to the quite strong interaction between PE matrix and SiO_2 nanoparticles may be the main reason for the increase in T_g values.

Mechanical Properties of NCs

Tensile properties of PE hybrids films were studied by typical stresse-strain curves of some hybrid membranes. Specific values of the ultimate properties and the modulus of these samples are listed in Table 3. In comparison with the pure PE, samples containing SiO_2 have higher ultimate strength; higher initial Young's modulus, but lower ultimate elongation. Filler consisting entirely of SiO_2 generally increases the ultimate strength, but decreases the maximum extensibility. Ultimate strength and initial modulus were increased with SiO_2 contents, but ultimate elongation decreased sharply with the increase of SiO_2 contents, especially at lower SiO_2 content. The strength should be reduced if there are no bonding sites between the matrix polymer phase and the inorganic SiO_2 phase. This is presumably due to the inert nature of the PE and the weak interactions between these polymers and the SiO_2. In this case, the SiO_2 acts as nonreactive, non-reinforcing filler. It is generally believed that external stress on a polymer composite is transferred from the continuous phase (polymer matrix) to the discontinuous phase (filler). Thus, the ultimate properties of the NCs are dependent on the extent of bonding between the two phases, the surface area of the SiO_2, and the arrangements between the SiO_2 particles. The above results showed that the interactions between the PE and the SiO_2 are very important [20].

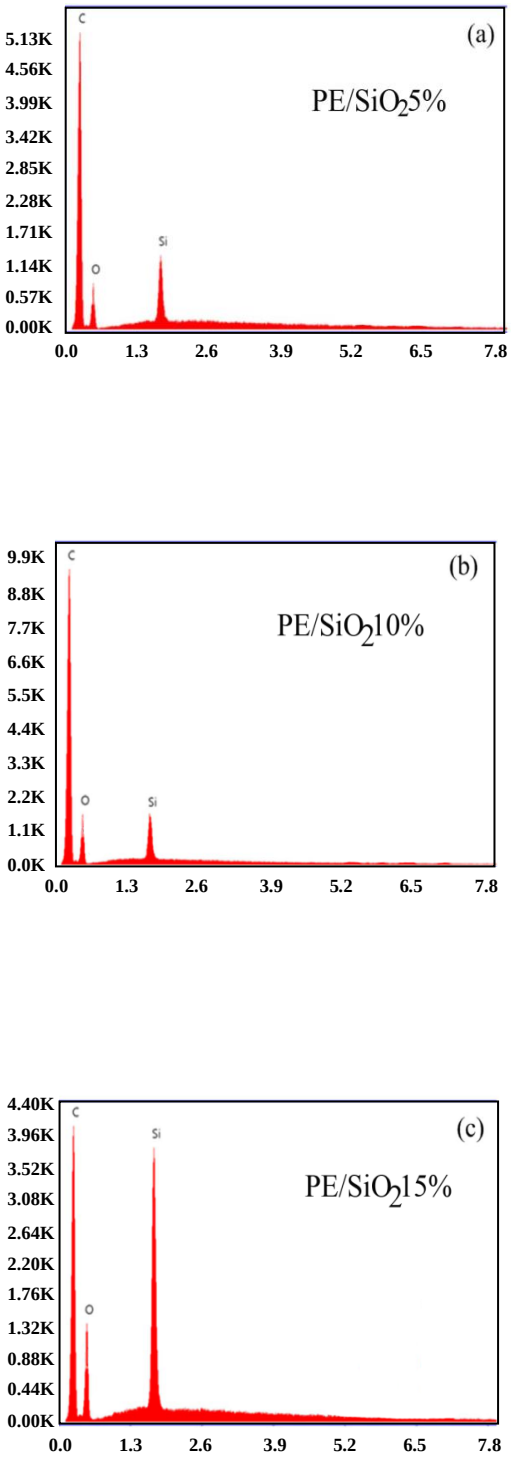

Fig. 2: EDS spectra of PE/SiO₂ composites with different SiO₂ contents: (a)5wt%, (b) 10wt%,(c)15wt%.

Morphology of NCs

Fig. 4 shown the particle size distribution of the PE/SiO_2. It can be observed that the particle size distribution of PE/SiO_2 (a) is relatively broad, from 60 nm to 300 nm. With increasing the PE content, the particle size became more uniform although the particle size distribution was not changed too much. There are four distribution peaks could be observed in Fig. 4b and only two distribution peaks emerged in Fig. 4c. These results show that the particle size distribution is affected by the content of PE. The particle size distribution became more uniform when more PE was added. However, it is notable that the distribution of particle size presents a certain extent multiple relationships. This multiple relationship could be attributed to the adhesion and/or aggregation among the particles. Commonly, the condensation of the TEOS is too fast to make a regular and well-proportioned self-assembly process under the alkaline condition, so the adhesion and aggregation would occur among the particles, and the bigger particles are usually composed of two or more small particles. Therefore, the multiple relationship of particle size was presented. The mean particle size of PE/SiO_2 could also be obtained by NTA measurements. The mean particle sizes of Figs. (a, b) and (c) were 68 nm, 72 nm and 80 nm respectively. It should be mentioned that the mean particle size obtained by NTA measurement is a statistical number which was calculated from a great number of particles, the density of particles tested in this paper was more than 80 particles/ml, therefore the mean particle size has a more average meaning. According to these particle size distribution and mean particle size results, it is reasonable to infer that the PE content would determine the mean size and uniformity of PE/SiO_2 to a certain extent. It has been found that the more PE was added, the more uniform and bigger mean size PE/SiO_2 particles could be obtained. The SEM observations of the PE/SiO_2 5% and 10% are presented in Fig. 5a and b. The surface morphology of the PE/SiO_2 shows that the nanocomposites were composed of particles of different shapes and sizes. These are no polymer that could be observed outside the particles, indicating that the polymer was located within the silica. It can be seen clearly that the particles possessed a non-uniform aggregation, some smaller particles were adhered together to form a big one, which could prove the multiple relationship of particle

Table 2: Thermal characterizations of PE/SiO_2 nanocomposite film.

Entry	Material	T_{10}[a] (ºC)	Char yield (%)[b]	T_g [c] (°C)
1	Pure PE	365	54	124.29
2	PE/SiO_2 (5%)	405	59	155.52
3	PE/SiO_2 (10%)	527	62	167.78
4	PE/SiO_2 (15%)	555	65	176.12

[a]*Temperature at which 10% weight loss was recorded by TGA at a heating rate of 10ºC/min in a nitrogen atmosphere.*
[b]*Percentage weight of material left undecomposed after TGA analysis at maximum temperature 800ºC in a nitrogen atmosphere*
[c]*Measured at a heating rate of 10 °C min^{-1} under N_2 atmosphere*

Table 3: Mechanical properties for PE with various SiO2 compositions.

Entry	Material	Modulus[a](MPa)	Ultimate strength[b](MPa)	Ultimate elongation[c](%)
1	Pure PE	2112.15	108.21	11.57
2	PE/SiO_2 (5%)	2643.21	118.28	9.35
3	PE/SiO_2 (10%)	2762.43	121.54	8.65
4	PE/SiO_2 (15%)	2925.14	128.12	7.53

[a]*Initial slope of the stress–strain curve.* [b]*Stress at break.*[c]*Elongation at break.*

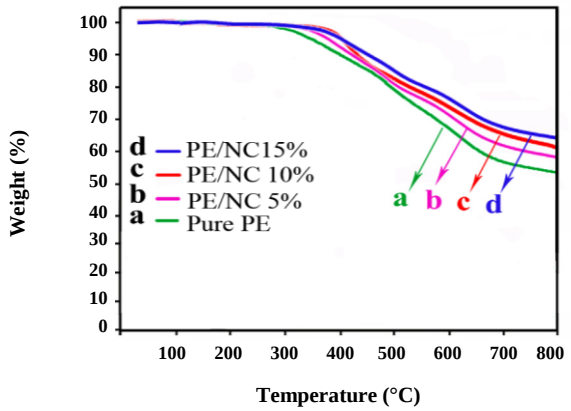

Fig. 3: TGA thermograms of pure PE (a) PE/SiO_2 NC 5%, (b) PE/SiO_2 NC 10%, (c) PE/SiO_2 NC 15%, (d).

size, as shown in Fig. 4. Commonly, the hydrolysis and condensation of TEOS are reported to promote the formation of a cross-linked structure [21, 22]. Therefore, the aggregations of particles could be attributed to the irregular self-assembly of TEOS. In addition, the relative high synthesis temperature would also disturb the self-assembly process of TEOS. It should be mentioned that some stripes could be observed on the surface of the particles. These stripes may be composed by silica, proved by the similar contrast with the silica matrix, as can be seen in Fig. 5c and d. The hydrolysis products of TEOS prefer inhabiting around the O atom in PE and formed a silica network to interact with the hydroxyl group at the end of the PE, which formed the irregular stripes on the surface of PE/SiO_2. So the hydrolysis and condensation products of TEOS in the water phase may be also attached on the silica matrix or form the conjoint silica residue among the particles. The TEM images present the structure information of PE/SiO_2. As shown in Fig. 5c and d, the adherence between the particles could be observed clearly. There is no typical hollow structure could be observed among the particles, indicating the PE/SiO_2 was not the core–shell structure. Considering that the polymer was located within the silica, as suggested by SEM images, it is reasonable to infer that the PE/SiO_2 may possess an interpenetrating structure, which confirmed by the TGA, DSC measurement results [22].

Gas permeation properties of PE/SiO2 nanocomposite membranes

Permeability and selectivity of pure gases through the membranes

The permeability of pure nitrogen, oxygen, methane and carbon dioxide gases was measured on the pure polymer and nanocomposite membranes of PE/SiO_2 at 10 barg and 25 °C. The results in Figs. 6(a) shown that the order of permeability of gases in both pure and composite membranes is as follows:

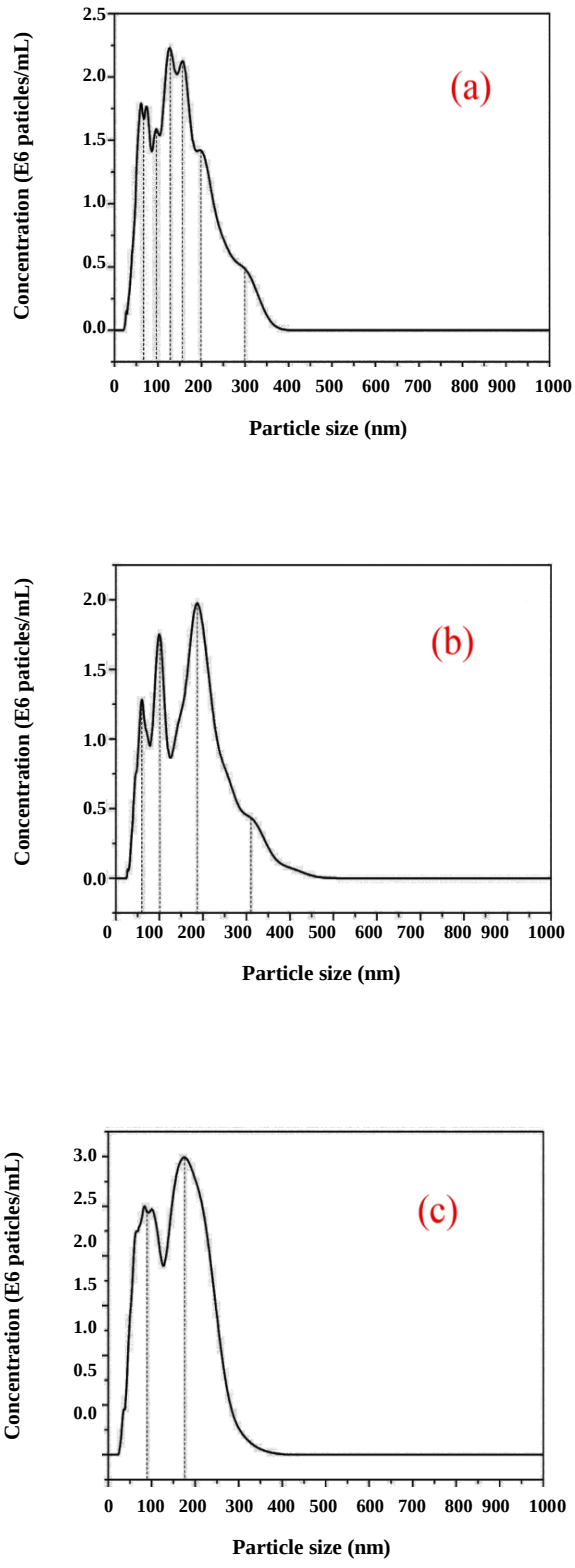

Fig. 4: Particle size distribution of the PE/SiO_2 NCs.

$P_{CH4}<P_{N2}<P_{O2}<P_{CO2}$

As known, permeation of molecules through polymeric membranes occurs via solution-diffusion mechanism. Considering that PE polymer is a conductive polymer, the process of gas separation on this polymer is performed based on domination of diffusion mechanism which can describe as molecular sieving. Table 4 reveals the investigations on the kinetic diameter of the relevant gases that the kinetic diameter of studied gases changes as follows:

$d_{CO2}<d_{O2}<d_{N2}<d_{CH4}$

The order of permeability of gases is exactly contrary to the kinetic diameters of studied gases. So, it was found that diffusion is the dominant mechanism in permeability of gases through the PE and PE/SiO_2 membranes, and the gases with smaller molecular size have the higher permeability in the membranes. As shown in Fig. 6a, the permeability of gases increased in the membranes by silica particles in PE. The permeability of carbon dioxide, methane, oxygen, and nitrogen increased from 0.124, 0.007, 0.035, and 0.008 barrer in pure polymer to 0.219, 0.016, 0.069 and 0.019 barrer, respectively, in PE/SiO_2 nanocomposite membranes containing 15 wt% silica nanoparticles. In general, the permeability of gases increases by the following order:

P_{CH4} (38%) <P_{N2} (58%) <P_{CO2} (88%) <P_{O2} (98%)

As observed in SEM and TEM image, the presence of silica particles results in two groups of particles. The first group consists of micro-size particles which have a weak interaction with the polymer matrix and their contacting surface with the polymer matrix is also weak; it creates a free space at the intersection of particles and polymer [24, 25]. The second group includes the nanoparticles with a good interaction with the polymer matrix and good bonds with the polymer chains. The free space created in the intersection between polymer and silica can provide the space needed for the movement of gas molecules in polymer matrix, and it provides more opportunities for transportation of gas molecules through the membrane. Therefore, the permeability increases by silica content of PE/SiO_2 membranes. Considerable increase in the permeability of carbon dioxide in comparison to other gases is related to structural changes occurring in the membranes. Such changes result from the presence

Table 4: The kinetic diameter and condensability of the relevant gases [23, 24].

Gas	Condensability temperature (K)	Kinetic diameter (Å)
CO_2	195	3.30
CH_4	149	3.80
O_2	107	3.46
N_2	71	3.64

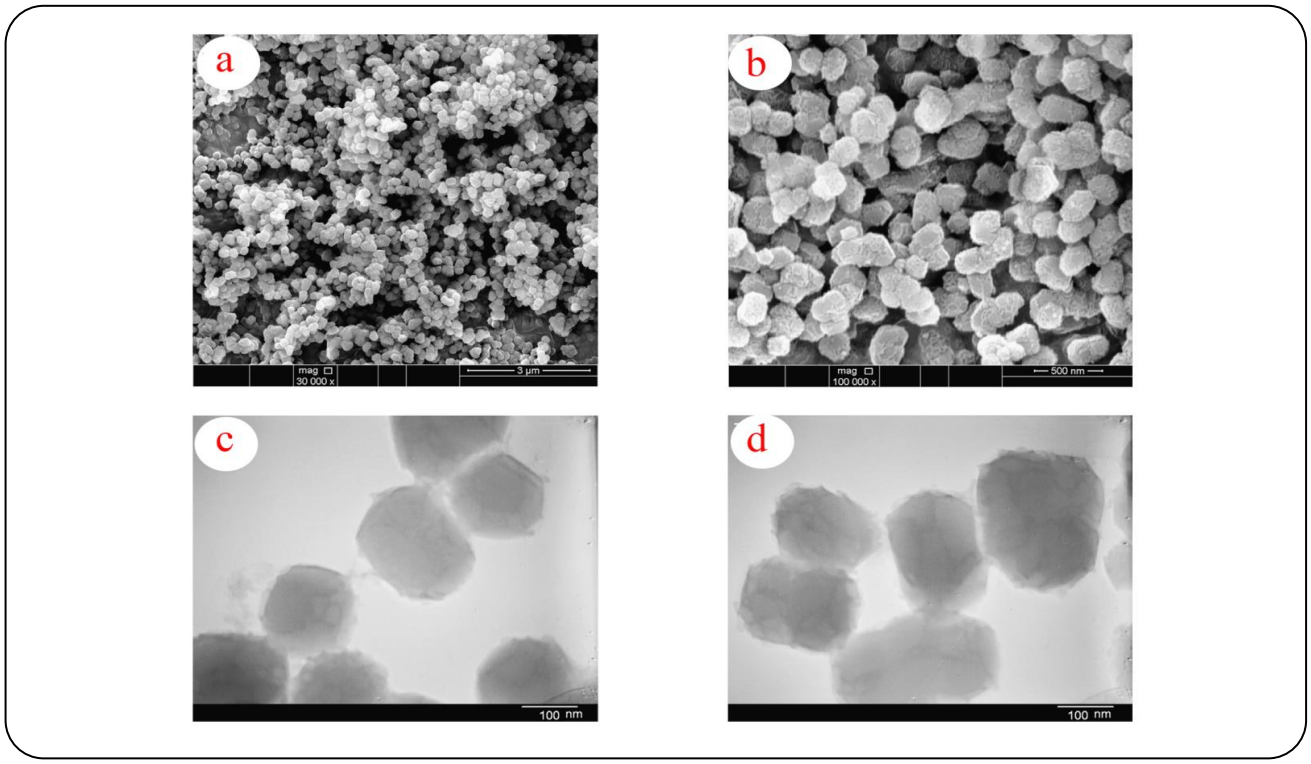

Fig. 5: SEM micrographs of PE/SiO_2 NC 5% (a) and PE/SiO_2 NC 10% (b) and TEM micrograph PE/SiO_2 NC 5%, (c), PE/SiO_2 NC 10%, (d).

of silica nanoparticles in the polymer matrix, leading to changes in the diffusion and solubility coefficient of gases in the polymer matrix. In the following, the reasons for such changes are investigated, stating the diffusion and solubility coefficients. Moreover, the increase in the free space enclosed by the polymer provides more suitable space for smaller gases to pass resulting in more increase in the permeability of smaller molecules. As shown in Fig. 5, the prepared membranes have dense structure with distributed nanospaces in the polymer particle interfaces. As a result, gas separation occurs based on solution-diffusion mechanism.

Fig. 6b shown the increment in selectivity of studied gases in nanocomposite membranes by silica. The selectivity of CO_2/N_2, CO_2/CH_4 and O_2/N_2 increases from 17.18, 16.66 and 4.20 to 20.08, 18.19 and 7.12 respectively, in nanocomposite membranes containing 15 wt% silica nanocomposite. As reported in the SEM and TEM analysis, addition of silica nanocomposites in polymer creates some free spaces at the polymer-agglomerated particles. These free spaces would enhance the diffusion and solution of gases in polymer. As reported in Table 5, by addition of silica nanoparticles to polymer the solubility selectivity of pair gases changes more than diffusivity selectivity. It is due to spaces created in the polymer-agglomerated silica interface which enhance the higher sorption of small gases in comparison to others and finally lead

Table 5: The solubility and diffusion selectivity for different gases at 25 °C and the feed pressure of 10 barg.

Membrane	Diffusivity selectivity			Solubility selectivity		
	D_{O2}/D_{N2}	D_{CO2}/D_{N2}	D_{CO2}/D_{CH4}	S_{O2}/S_{N2}	S_{CO2}/S_{N2}	S_{CO2}/S_{CH4}
Pure s-PBI	4.09	3.28	3.47	3.78	19.84	9.54
PE/SiO2 (5%)	4.58	3.25	3.36	3.68	21.69	10.24
PE/SiO2 (10%)	4.69	3.27	3.29	3.59	24.88	9.88
PE/SiO2 (15%)	4.88	3.22	3.18	3.61	27.34	12.56

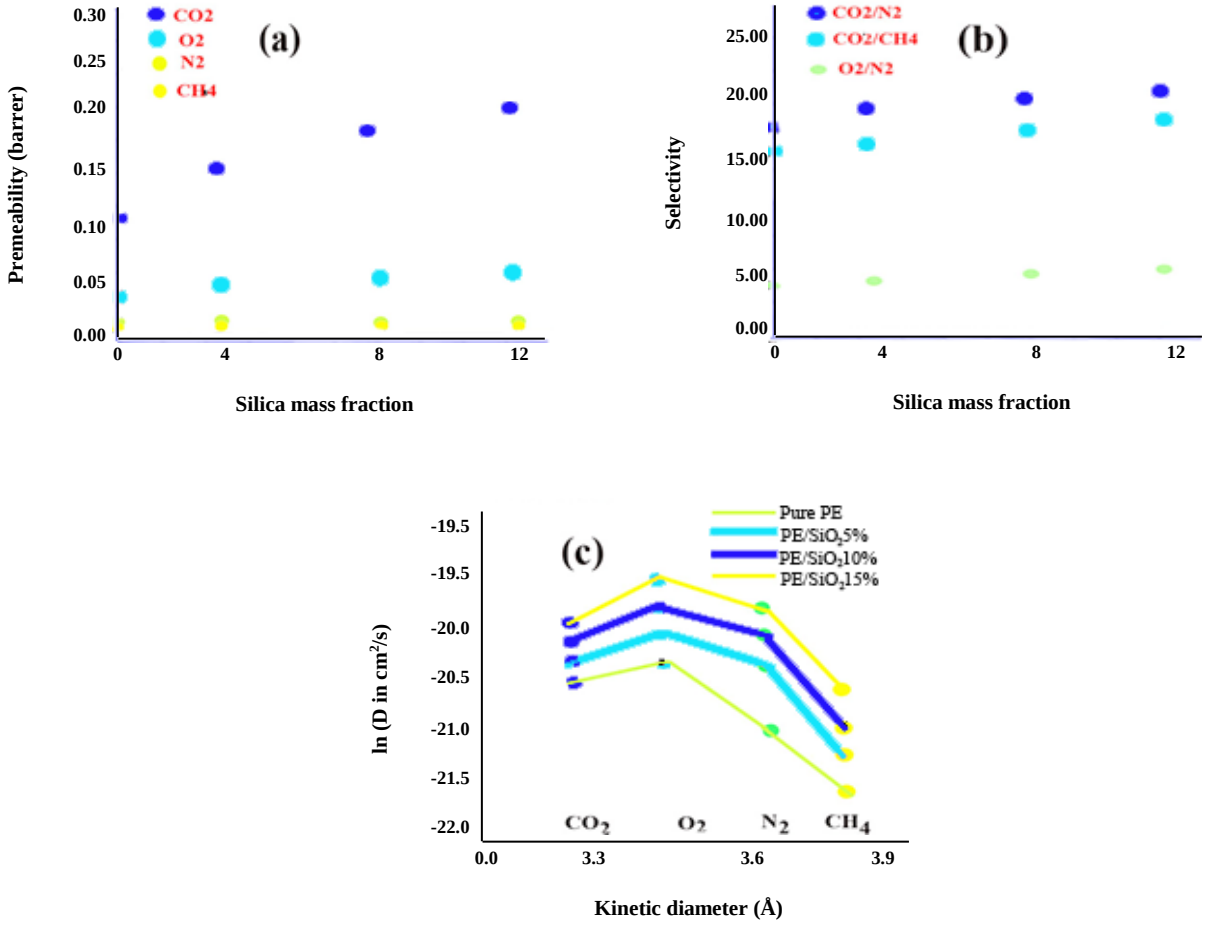

Fig. 6: (a) Gas permeability of membranes at 25 °C and the feed pressure of 10 barg, (b) CO_2/N_2, CO_2/CH_4 and O_2/N ideal selectivities of prepared nanocomposite membranes and (c) Correlation of diffusion coefficients to kinetic diameter of gases in composite membranes.

to higher gas selectivity in polymer. Also, the results in Fig. 6b indicate the higher increment in the selectivity of CO_2/N_2 and CO_2/CH_4 pair gases compared to that of O_2/N_2. It is because of the increase in the solubility selectivity of carbon dioxide compared to nitrogen and methane, which will be discussed in the section dealing with the solubility coefficients. To evaluate the effect of silica nanoparticles in enhancing gas separation properties of PE/SiO_2 membranes.

Effect of adding silica nanoparticles on diffusion and solubility coefficients of gases

Table 5 shown the diffusion coefficient of different gases in the nanocomposite membranes. This figure indicates that the diffusion coefficients of all gases increase by the silica in the nanocomposite membranes. Also, it is clear that the changes in the diffusion coefficient of gases in pure polymer and nanocomposite membranes are as follows:

$$D_{CH4}<D_{N2}<D_{CO2}<D_{O2}$$

As it is obvious, the diffusion into the polymer is characterized by the molecular size, which is in turn determined by the kinetic diameter. The kinetic diameter is calculated only by the minimum diameter of the molecule profile and only indicates the minimum diameter needed for molecule to penetrate without considering the length of penetrating molecule. So, the diameter establishes a suitable relation with the penetration rate of the short molecules such as gas molecules including oxygen, nitrogen, and methane. Based on the diffusion theory, a gas molecule can penetrate when Brownian movement of the polymer chains provides enough space. This required space depends on the minimum cross-section and the length of penetrating molecule. This can serve as a reason for the linear relation between log D and the kinetic diameter of gas molecules, shown in Fig. 6c for pure PE and PE/SiO_2 nanocomposite membranes. As shown in Fig. 6c, carbon dioxide does not behave like other gases, and unlike what is expected for oxygen, its permeability does not decrease with the reduction in the kinetic diameter. This can be because the carbon dioxide molecule is non-spherical and it has the double bond in its structure that prevents it from penetrating through the membrane [24, 26].

Solubility Coefficients

As it is clear, the gas sorption in polymeric membranes depends on the condensability of gases, interaction between the polymer and gas molecules, the structure of the polymer, temperature and pressure. The presence of an electron cloud on the double bond of carbon dioxide results in the increase in the instant bipolarity, and consequently better interaction of this molecule with polymer bonds. In addition to the above-mentioned reasons, it is easier for carbon dioxide to enter the free volumes in the polymer structure because of its smaller molecular size.

Table 5 shown the changes in the solubility coefficient of various gases in nanocomposite membranes. Considering above and the results given in Table 5, the order for solubility coefficient in the investigated membranes is as follows:

$$S_{CO2}>S_{CH4}>S_{O2}>S_{N2}$$

According to the obtained results, the solubility of gases increases based on their condensability. The presence of silica particles results in the increase in the density of polar groups of OH in the polymer matrix, and consequently in the establishment of the polar spaces at the intersection of the particles and the polymer. Polar spaces result in an increase in the solubility coefficient of condensable gases. The solubility coefficient of carbon dioxide increases more than that of methane because of its polarity, and as a result, the possibility of formation of polar bonds with the polar groups. Table 6 shown the solubility and diffusion selectivity for different gases at 25 °C and the feed pressure of 10 barg. Considering Table 5, after adding silica nanoparticles, the solubility selectivity as well as its effect on the ideal selectivity will increase because of the increase in the solubility coefficient of carbon dioxide.

nanocomposite membranes and (c) Correlation of diffusion coefficients to kinetic diameter of gases in composite membranes.

CONCLUSIONS

In summary, a new thermally stable and PE was synthesized by direct step-growth polycondensation. Ultrasonic process was applied as a profitable route for synthesis of the PE/SiO_2 NCs. PE/SiO_2 nanocomposite membranes were prepared succesfully by introducing nanosized SiO_2 particles in a polyester polymer network to investigate the effect of nanofiller on the morphology, thermal stability and gas transport properties. The results of the permeation investigation of PE/SiO_2 nanocomposite membranes show that addition of SiO_2 enhances the gas permeability of polyester with increasing nanoparticles content. This behavior results from an increase in free volume because of the inefficient chain packing, as well as the presence of extra void volume at the interface between polymer and SiO_2

nanoparticles. TEM analysis showed dispersion of SiO_2 with average particle sizes about 16 nm in the polymer matrix. Also, morphological study of synthesized NCs exhibited the SiO_2 nanoparticles mostly dispersed homogeneously on the polymer matrix by FE-SEM analysis.

Received : Jan. 1, 2019 ; Accepted : Nov. 18, 2019

REFERENCES

[1] Shao L., Low B.T., Chung T.S., Greenberg A.R., Polymeric Membranes for the Hydrogen Economy: Contemporary Approaches and Prospects for the Future, *J. Membr. Sci*. **327**: 18-31 (2009).

[2] Ahmadizadegan H., Esmaielzadeh S., Ranjbar M., Improving the Proton Conductivity and Antibacterial Properties of Sulfonated Polybenzimidazole/ZnO/Cellulose with Surface Functionalized Cellulose/ZnO Bionanocomposites. *Iranian Journal of Chemistry and Chemical Engineering (IJCCE)*, **37**: 27-42 (2018).

[3] Salimi M., Pirouzfar V.,Kianfar E., Enhanced Gas Transport Properties in Silica Nanoparticle Filler-Polystyrene Nanocomposite Membranes, *Colloid Polym Sci* **295**: 215–226 (2017).

[4] Le Baron P.C., Wang Z., Pinnavala T.J., Polymer Layered Silicate Nanocomposites an Overview *Appl.Clay.Sci*, **15**: 11-29 (1999).

[5] Moqadam S., Salami Kalajahi M., Mahdavian M., Synthesis and Characterization of Sunflower Oil-Based Polysulfide Polymer/Cloisite 30B Nanocomposites. *Iranian Journal of Chemistry and Chemical Engineering (IJCCE)*, **37**: 185-192 (2018).

[6] Jing L., Wang W.W., Wel X., Wu D., Jin R., Effects of Water on the Preparation, Morphology and Properties of Polyimide and Silica Nano Composite Films Prepared by Sol-Gel Process, *J. Appl Polym. Sci*., **104**: 1579-1586, (2007).

[7] Ghorpade R.V., Rajan C.R., Chavan N.N., Ponrathnam S., Synthesis of Novel Silica-Polyimide Nanocomposite Films Using Aromatic-Amino Modified Silica Nanoparticles: Mechanical, Thermal and Morphological Investigations, eXPRESS *Polymer Letters*.**9**: 469–479 (2015).

[8] Chitra B., Sathish K., K. Sonication Effects on Stability and Thermal Properties of Silica- Paraflu Based Nanofluids. *Iranian Journal of Chemistry and Chemical Engineering (IJCCE)*, **36**: 153-159 (2017).

[9] Timur, M., Demetgül, C. Synthesis and Metal Ion Uptake Studies of Silica Gel-Immobilized Schiff Base Derivatives and Catalytic Behaviors of their Cu(II) Complexes. *Iranian Journal of Chemistry and Chemical Engineering (IJCCE)*, **36**: 111-122 (2017).

[10] Kawasumi M, Masegawa N K, Ato M ,Uskd A and Okada A, Preparation and Mechanical Properties of Poly Propylene Hybrids, *Macromolecules*, **30**: 6333-6338 (1997).

[11] Ahmadizadegan H., Esmaielzadeh S., Fabrication and Characterization of Novel Polyester Thin-Film Nanocomposite Membranes Achieved by Functionalized SiO_2 Nanoparticles for Gas Separation, *Polym Eng Sci*., **59**: 237-247 (2019).

[12] Ahmadizadegan H., Esmaielzadeh S., Novel polyester/SiO_2 Nanocomposite Membranes: Synthesis, Properties and Morphological Studies, *Solid State Sciences*, **80**: 81-91 (2018).

[13] Hu Q., Marand E., Dhingra S., Fritsch D., Wen J., Wilkes G. Poly(amide-imide)/TiO_2 Nano-Composite Gas Separation Membranes: Fabrication and Characterization, *J. Membr. Sci*, **135**: 65-79 (1997).

[14] Ahmadizadegan H., Synthesis and Gas Transport Properties of Novel Functional Polyimide/ZnO Nanocomposite thin Film Membranes, *RSC Adv*., **6**: 106778-106789 (2016).

[15] Li T., Liu J., Zhao Sh., Chen Zh., Huang H., Guo R., Chen Y., Microporous Polyimides Containing Bulky Tetra- O -Isopropyl and Naphthalene Groups for Gas Separation Membranes, *Journal of Membrane Science*, **585**: 282-288 (2019).

[16] Ahmadizadegan H., Esmaielzadeh Sh., Ranjbar M., Marzban Z., Ghavas F., Synthesis and Characterization of Polyester Bionanocomposite Membrane With Ultrasonic Irradiation Process For Gas Permeation and Antibacterial Activity, *Ultrason. Sonochem*. **41**: 538–550 (2018).

[17] Ahmadizadegan H., Khajavian R., Novel Functional Aromatic Polyimides and Polyimide/Titania Nanocomposite Thin Films for Gas Separation: Preparation and Structural Characterization, *J. Iran. Chem. Soc*. **14**: 777–789 (2017).

[18] Yuanliang Zhao; Xiaowen Qi; Yu Dong; Jian Ma; Qinglong Zhang; Laizhou Song; Yulin Yang; Qingxiang Yang, Mechanical, Thermal and Tribological Properties of Polyimide/Nano-SiO_2 Composites Synthesized Using an In-Situ Polymerization, *Tribology International* **103**: 599-608 (2016).

[19] Toiserkani H., Polyimide/Nano-Tio_2 Hybrid Films Having Benzoxazole Pendentgroups: in Situ Sol–Gel Preparation and Evaluation of Properties, *Progress in Organic Coatings* **88**: 17–22 (2015).

[20] Seyedjamali H., Pirisedigh A., Synthesis of Well-Dispersed Polyimide/TiO_2 Nanohybrid Films Using a Pyridine-Containing Aromatic Diamine, *Polym. Bull*. **68**: 299–308 (2012).

[21] Chen B., Chiu T., Tsay S., Synthesis and Characterization of Polyimide/Silica Hybrid Nanocomposites, *J. Appl. Polym. Sci*. **94:** 382 (2004).

[22] Zu L., Li R., Jin L., Lian H., Liu Y., Cui X., Preparation and Characterization of Polypropylene/Silica Composite Particle with Interpenetrating Network Via Hot Emulsion Sol–Gel Approach, *Progress in Natural Science: Materials International* **24**: 42-49 (2014).

[23] Kong Y., Du H., Yang J., Shi D., Wang Y., Zhang Y., Xin W., Study on Polyimide/TiO_2 Nanocomposite Membranes for Gas Separation, *Desalination*, **146**: 49–55 (2002).

[24] Ahmadizadegan H., Esmaielzadeh S., Gas Transport Membranes Based on Novel Optically Active Polyester/Cellulose/Zno Bionanocomposite Membranes, *J Iran Chem Soc* **15**: 799–811 (2018).

[25] Tena A., Fernández A.M., Viuda M., Palacio L., Prádanos P., Lozano A.E., Abajo J., Hernández A., Advances In The Design of Co-Poly(Ether-Imide) Membranes for CO_2 Separations. Influence of Aromatic Rigidity on Crystallinity, Phase Segregation and Gas Transport, *Eur. Polym. J.* **62**:130-138 (2015).

[26] Lua A.C., Shen Y., Preparation and Characterization of Polyimide–Silica Composite Membranes and Their Derived Carbon–Silica Composite Membranes for Gas Separation, *Chem. Eng. J*. **220**: 441–451 (2013).